Synthesis and Characterization of Hydrotalcites Containing Ni(II) and Fe(III) and Their Calcination Products

M. del Arco,[†] P. Malet,[‡] R. Trujillano,[†] and V. Rives*,[†]

Departamento de Química Inorgánica, Universidad de Salamanca, Salamanca, Spain, and Departamento de Química Inorgánica-Instituto de Ciencia de Materiales de Sevilla, Universidad de Sevilla-C.S.I.C., Sevilla, Spain

Received July 13, 1998. Revised Manuscript Received December 8, 1998

A layered double hydroxide with the hydrotalcite-like structure containing Ni(II) and Fe(III) cations in the brucite-like layers with the formula $[Ni_{0.7}Fe_{0.3}(OH)_2](CO_3)_{0.15}\cdot 0.94\ H_2O$ has been prepared by coprecipitation. On hydrothermal treatment, a coproduct, identified as a $NiFe_2O_4$ spinel, is formed. Both samples, as well as the solids obtained from them by calcination at 450 °C (where only mixed oxides are present) and 750 °C (where crystallization of well defined phases has taken place), have been characterized by powder X-ray diffraction (PXRD), X-ray absorption (XAS) and FT-IR spectroscopies, thermal analysis (differential and thermogravimetric), temperature-programmed reduction, and specific surface area assessment. XAS results show that in both calcined samples all Ni(II) cations are in octahedral holes, while Fe(III) cations are equally distributed between octahedral and tetrahedral holes. For the sample calcined at 750 °C, coordination parameters at the first and second shells of Ni(II) and Fe(III) cations coincide with those expected for a mixture of NiO and the $NiFe_2O_4$ spinel, in agreement with the detection of both crystalline compounds by PXRD. Although PXRD only detects crystalline NiO in the sample calcined at 450 °C, the presence of Fe(III) cations in tetrahedral holes discards the formation of a Ni(II)−Fe(III) oxide solid solution with a rock salt structure, thus indicating that Fe(III) ions are forming an amorphous phase at this temperature. In this sample, coordination parameters at the second shell of Fe(III) are also different from those expected for a spinel-like structure. In agreement with the experimental data, a structure for the cluster present in the amorphous phase is proposed. Reducibility of cations in the sample calcined at 450 °C depends on the synthesis method and on the formation of spinel-like nuclei.

Introduction

Hydrotalcite-like compounds, also called anionic clays or layered double hydroxides (LDH), have the formula $[M^{II}_{1-x}M^{III}_x(OH)_2](CO_3)_{x/2}\cdot nH_2O$. Metallic cations are located in coplanar octahedra $[M(OH)_6]$ sharing vertices and forming $M(OH)_2$ layers with the brucite (cadmium iodide-like) structure. The partial substitution of the divalent cations by trivalent ones involves a positive charge of the layer, balanced by anions between the hydroxylated layers, where water molecules also exist. A large number of LDHs have been synthesized with divalent cations such as Mg, Mn, Fe, Co, Ni, Cu, Zn, and Ca and trivalent cations such as Al, Cr, Mn, Fe, Co, La, and Y. The same structure is also found in some compounds with the monovalent−trivalent association, as Li−Al.[1−4] In the same way, it is possible to synthesize LDHs containing three or more cations in the layers.[5−8] Intercalation of a great variety of anions (halides, complex anions, polyoxometalates, etc.) between the brucite-like layers is also possible. The structure and arrangement of the cations in the brucite-like layer in these materials, as well as the structure of the solids obtained after calcination of hydrotalcites and their decomposition mechanism, have been widely studied in the literature.[6,9−11]

Lamellar compounds with hydrotalcite-like structures have been used as ion exchangers,[12−14] catalysts, and catalyst precursor after being calcined at fixed temper-

[†] Universidad de Salamanca.
[‡] Universidad de Sevilla-C.S.I.C.

(1) Serna, C. J.; Rendon, J. L.; Iglesias, J. E. *Clays Clay Miner.* **1982**, *30*, 180.
(2) Twu, J.; Dutta, P. K. *Phys. Chem.* **1989**, *93*, 2592.
(3) Chisem, I.; Jones, W. *J. Mater. Chem.* **1994**, *4*, 1727.
(4) Chisem, I.; Jones, W.; Martín, C.; Martín, I.; Rives, V. *J. Mater. Chem.* **1998**, *8*, 1917.
(5) Morpurgo, S.; Lo Jacono, M.; Porta, P. *J. Solid State Chem.* **1995**, *119*, 246.
(6) Porta, P.; Morpurgo, S.; Pettiti, I. *J. Solid State Chem.* **1996**, *121*, 372.
(7) Barriga, C.; Kooli, F.; Rives, V.; Ulibarri, M. A. In *Synthesis of Porous Materials: Zeolites, Clays and Nanostructures;* Occelli, M. L., Kessler, H., Eds.; Marcel Dekker: Nueva York, 1996; Chapter 41, p 661.
(8) Kooli, F.; Kosuge, K.; Tsunashima, A. *J. Solid. State Chem.* **1996**, *118*, 285.
(9) Belloto, M.; Rebours, B.; Clause, O.; Lynch, J.; Bazin, D.; Elkaim, E. *J. Phys. Chem.* **1996**, *100*, 8527.
(10) Labajos, F. M.; Rives, V.; Malet, P.; Centeno, M. A.; Ulibarri, M. A. *Inorg. Chem.* **1996**, *35*, 1154.
(11) Del Arco, M.; Rives, V.; Trujillano, R.; Malet, P. *J. Mater. Chem.* **1996**, *6*, 1419.
(12) Miyata, S. *Clays Clay Miner.* **1983**, *31*, 305.
(13) Schutz, A.; Biloen, P. *J. Solid State Chem.* **1987**, *68*, 360.

10.1021/cm9804923 CCC: $18.00
Published on Web 02/20/1999

atures. Transition metals and their oxides are widely used as catalysts; the successful synthesis of multicomponent catalysts usually requires a homogeneous dispersion of the components; the use of hydrotalcites (where the cations are well-dispersed in the brucite-like layers) ensures the formation of well-dispersed oxides with a prearranged ratio of the metals.

Ni−Fe hydroxycarbonate exists as the mineral reevesite,[15,16] and it has been also synthesized;[17,18] it possesses the hydrotalcite-like structure, although the monometallic hydroxycarbonates are amorphous. This material could be a good precursor for CO hydrogenation catalysts after decomposition and reduction. In the present paper, we report on the synthesis and characterization of lamellar hydroxycarbonates containing Ni^{2+} and Fe^{3+}, prepared by a coprecipitation method. The samples thus obtained have been calcined at different temperatures to yield NiFe mixed oxides. The samples have been characterized by PXRD, EXAFS/XANES, FT-IR, DTA, TG, TPR, and specific surface area measurements.

Experimental Section

Samples Preparation. Solution A was obtained by dissolving 9.34 g of NaOH (ca. 0.233 mol) and 7.3 g of Na_2CO_3 (ca. 0.0687 mol) in 200 mL of distilled water. Solution B was prepared by dissolving 20 g of $Ni(NO_3)_2{\cdot}6H_2O$ (ca. 0.0687 mol) and 13.89 g of $Fe(NO_3)_3{\cdot}9H_2O$ (ca. 0.0344 mol) in 200 mL of distilled water. While solution A was being vigorously, magnetically stirred, solution B was added dropwise (ca. 30 drops/min) from a separation funnel at room temperature (ca. 25 °C). An ochreous suspension was obtained. After completing the addition of solution B, the mixture was stirred for 2 h. The suspension obtained was split in two portions: sample NiFe corresponds to the solid isolated from the suspension, after stirring at 50 °C during 2 days, while sample NiFeH corresponds to the solid isolated after submitting the suspension to hydrothermal treatment at 100 °C during 6 days in a Teflon-lined, stainless steel bomb, at autogenous pressure. The solids were isolated in both cases by filtration and washed until no nitrate ions were detected in the washing liquids.[19]

As shown below, calcination in air of these samples led to weight loss up to ca. 425 °C. For this reason, the samples were calcined in air at 450 °C (that is, after completing the weight loss) or 750 °C (when well-crystallized phases are expected to be formed) during 3 h, to yield samples NiFe-*T* or NiFeH-*T*, were *T* stands for the calcination temperature, in degress Celsius.

Techniques. Chemical analysis for nickel and iron were carried out by atomic absorption in a Mark-II ELL-240 instrument. Powder X-ray diffraction (PXRD) diagrams were recorded in a Siemens D-500 apparatus, using Cu Kα radiation, connected to a DACO-MP microprocessor with Difract/AT software. Differential thermal analysis (DTA) and thermogravimetric analysis (TG) were recorded in air in DTA-1700 and TGS-2 instruments, respectively, from Perkin-Elmer, connected to a Perkin-Elmer 3600 data station, at a heating rate of 10 °C min^{-1}. The Fourier transform infrared spectra (FT-IR) were recorded in a FT-IR 1730 Perkin Instrument using the KBr pellet technique; 100 scans were averaged, with a nominal resolution of 4 cm^{-1}. Specific surface area and porosity assessment was carried out from the nitrogen adsorption isotherms at 77 K, measured in a conventional high-vacuum system, provided with a silicon oil diffusion pump, McLeod gauge, grease-free stopcocks, and a Baratron MKS pressure transducer; analysis of the isotherms was performed with the assistance of a computer program described elsewhere.[20] Temperature-programmed reduction (TPR) analysis was carried out in a Micromeritics TPR/TPD 2900 instrument, at a heating rate of 10 °C min^{-1}, and using ca. 10 mg of sample and a H_2/Ar (5% vol) mixture (from Sociedad Española del Oxígeno) as reducing agent (60 mL min^{-1}). Experimental conditions for TPR runs were chosen according to data reported elsewhere[21] in order to attain good resolution of component peaks; calibration was carried out from reduction of CuO (from Merck). Room temperature X-ray absorption spectra (XAS) at the iron and nickel K-edges were recorded in transmission mode at station XAS III at the LURE-DCI storage ring (Orsay, France), using optimized ion chambers as detectors. Monochromatization was achieved with a double silicon crystal working at the (311) reflection, detuned 20% to reduce higher harmonics. Samples were kept in place with Kapton sellotape, using amounts previously calculated to get total absorption coefficients close to 2.5, just above the absorption edge, and edge jumps $\Delta\mu_x \approx 1$. Five scans were recorded and averaged to get the final absorption spectra. The EXAFS function $\chi(k)$ was obtained from the experimental XAS spectrum by conventional procedures.[22] Theoretical backscattering amplitude and phase shift functions for absorber−backscatterer pairs were calculated by using the program FEFF.[23] EXAFS data analysis and handling were performed by using the program package XDAP.[24] Comparison among different models used percent variance values calculated as

$$V = \frac{\int_{k_{min}}^{k_{max}} [k^3(\chi_{model}(k) - \chi_{exp}(k))]^2 \, dk}{\int_{k_{min}}^{k_{max}} [k^3\chi_{exp}(k)]^2 \, dk} \times 100$$

and the goodness of fit parameter, ϵ_ν^2, calculated as described by Lytle et al.[25]

$$\epsilon_\nu^2 = \frac{\nu}{N_p(\nu - N_f)} \sum_{i=1}^{N_p} \frac{[\chi_{model,i} - \chi_{exp,i}]^2}{\sigma^2}$$

N_p being the number of experimental data, N_f the number of free parameters, ν the number of degrees of freedom ($2\Delta k\Delta R/\pi + 1$) and σ the average error in experimental data, taken as 10^{-3}.

Results and Discussion

Elemental Chemical Analyses. Values from elemental chemical analyses for the metals are given in Table 1 for the original samples. Although in some cases it has been reported that the metal molar ratio in hydrotalcites is close to the value in the starting solutions,[26,27] in this case the M^{2+}/M^{3+} value is larger than in the starting solutions (ca. 2.0). Moreover, after

(14) Chibwe, K.; Valim, J. B.; Jones, W. In *Proceedings from the Symposium on New Catalytic Materials and Techniques*, ACS Meeting, Division of Petroleum Chemistry, Miami, FL, 1989, p 507.
(15) De Waal, S. A.; Viljoen, E. A. *Am. Miner.* **1971**, *56*, 1007.
(16) Bish, D. L.; Livingstone, A. *Miner. Magn.* **1981**, *44*, 339.
(17) Sato, T.; Fujita, H.; Endo, T.; Shimada, M.; Tsunashima, A. *Reactivity Solids* **1988**, *5*, 219.
(18) Uzunova, E.; Klissurski, D.; Kassabov, S. *J. Mater. Chem.* **1994**, *4*, 153.
(19) Burriel, F.; Lucena, F.; Arribas, S.; Hernández, J. *Química Analítica Cuantitativa*, 13th ed.; Paraninfo: Madrid, 1989.
(20) Rives, V. *Adsorption Sci. Tech.* **1991**, *8*, 95.
(21) Rives, V.; Ulibarri, M. A.; Montero, A. *Appl. Clay Sci.* **1995**, *10*, 83.
(22) Sayers, D. E.; Bunker, B. A. In *X-ray Absorption: Principles of EXAFS, SEXAFS and XANES*; Koningsberger, D. C.; Prins, R., Eds.; Wiley: New York, 1988.
(23) Mustre de Leon, J.; Rehr, J. J.; Zabinky, S. I.; Albers, R. C. *Phys Rev. B* **1991**, *44*, 4146.
(24) A complete description of this program can be found at URL http://www.xs4all.nl.
(25) Lytle, F. W.; Sayers, D. E.; Stern, E. A. *Physica B* **1989**, *158*, 701.
(26) Cavani, F.; Trifiro, F.; Vaccari, A. *Catal. Today* **1991**, *11*, 173.

Table 1. Elemental Chemical Analyses Results for the Initial Samples, Assuming a Formula $[Ni_{1-x}Fe_x(OH)_2](CO_3)_{x/2}\cdot nH_2O$

sample	%Ni[a]	%Fe[a]	x	Ni/Fe[b]	n[c]	S_{BET}[d]
NiFe	35.1	14.1	0.30	2.38	0.94	94
NiFeH	39.3	12.6	0.25	2.97	0.68	24

[a] Weight percentage. [b] Molar ratio. [c] From TG analysis. [d] In m^2/g.

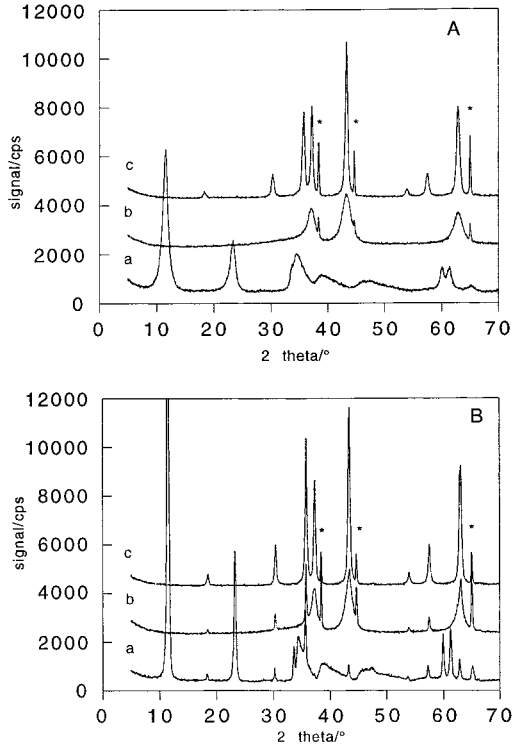

Figure 1. X-ray diffraction profiles of samples (A) NiFe, and (B) NiFeH. Traces correspond to the original sample (a) and sample calcined at 450 °C (b) and 750 °C (c). Signals denoted with an * correspond to the Al sampleholder.

thermal treatment, such a value is even larger than in the sample not submitted to hydrothermal treatment. In any case, the values here obtained are similar to those reported by Uzunova et al.[18] for hydrotalcites containing Ni^{2+} and Fe^{3+}.

X-ray Diffraction, X-ray Absorption Spectroscopies (XANES and EXAFS) and Specific Surface Area. *X-ray Diffraction*. X-ray diffraction diagrams for the initial samples are shown in Figure 1. Positions (in Å) of the maxima and their ascription to the corresponding (*hkl*) planes are given in Table 2.

The cell constant c is commonly calculated as $c = 3 \times d(003)$, assuming a 3R polytipism for the hydrotalcite,[29,30] while the value of cell constant a is calculated as $a = 2 \times d(110)$.[26] However, it has been proposed[31] that c can be better determined by averaging the

Table 2. Summary of PXRD Results for the Initial Samples[a]

NiFe		NiFeH			(*hkl*)	
expl	calcd	expl	calcd	ref 18	hydrotalcite	spinel
7.669	7.653	7.717	7.691	7.50	(003)	
		4.826	4.806			(111)
3.818	3.826	3.832	3.845	3.74	(006)	
		2.956	2.943			(220)
	2.648	2.661	2.651	2.64	(101)	
2.593	2.597	2.587	2.600	2.58	(012)	
	2.551		2.564		(009)	
		2.525	2.510	2.50		(311)
		2.412	2.403			(222)
2.307	2.305	2.321	2.310	2.30	(015)	
		2.090	2.081			(400)
1.954	1.953	1.920	1.959	1.93	(018)	
		1.710	1.699	1.71	(10*10*)	(422)
		1.608	1.602	1.62	(10*11*)	(511), (333)
1.539	1.539	1.541	1.541	1.53	(110)	
1.512	1.509	1.511	1.511	1.50	(113)	
		1.476	1.472		(10*13*)	(440)
1.429	1.428	1.430	1.430		(116)	
		1.410	1.407			(531)

[a] All values in Å. Sample NiFe: $a = 3.078$ Å, $c = 22.958$ Å. Sample NiFeH: $a = 3.082$ Å, $c = 23.072$ Å. Spinel:[28] $a = 8.325$ Å.

positions of diffraction peaks corresponding to planes (003) and (006) and even that of (009), if it is well defined and sharp, according to the formula

$$c/3 = {}^1/_2\{d(003) + [2 \times d(006)]\} \quad \text{or}$$
$$c/3 = {}^1/_3\{d(003) + [2 \times d(006)] + [3 \times d(009)]\}$$

In our case, we have used only the positions of the first two sharp peaks, as the third one, corresponding to planes (009), is rather broad and its position cannot be determined with sufficient precission. By using this method, the value calculated for c was 22.50 Å, while the value for parameter a was 3.08 Å, the differences between the values for both samples being within experimental error.

Ascription of the diffraction lines to the planes given in Table 2 has been done by assuming the calculated values for c and a and using the formula

$$[1/d^2] = [4(h^2 + hk + k^2)/3a^2] + [l^2/c^2]$$

for a polytipism 3R.[32] However, in the PXRD diagram of sample NiFeH, some lines cannot be ascribed to the hydrotalcite structure and, from data for the calcined samples (see below), it was concluded that they correspond to a $NiFe_2O_4$ spinel phase. This was confirmed by ascription of these diffraction peaks to the spinel phase using the formula

$$[1/d^2] = (h^2 + k^2 + l^2)/a^2$$

for the spinel phase (cubic). Values for c and a were calculated as above indicated, while the value for a for the $NiFe_2O_4$ spinel was taken from Greenwood.[28] In the same table a column has been inserted with the spacing values reported by Uzunova et al.[18] for a Ni−Fe hydrotalcite.

(27) De Roy, A.; Forano, C.; El Malki, K.; Besse, J. P. In *Expanded Clays and Other Microporous Solids, Synthesis of Microporous Materials;* Occelli, M. L., Robson, H., Eds.; van Nostrand Reinhold: New York, 1992, Chapter 7, p 108.
(28) Greenwood, N. N. *Cristales Iónicos, Defectos Reticulares y no Estequiometría*, 1st ed.; Editorial Alhambra, S. A.: Madrid, 1970.
(29) Bookin, A. S.; Cherkashin, V. I.; Drits, A. *Clays Clay Miner.* **1993**, *41*, 558.
(30) Bookin, A. S.; Drits, A. *Clays Clay Miner.* **1993**, *41*, 551.
(31) Ulibarri, M. A.; Labajos, F. M.; Rives, V.; Trujillano, R.; Kagunya, W.; Jones, W. *Inorg. Chem.* **1994**, *33*, 2592.
(32) Gay, P. *The Crystalline State. An Introduction*, 3rd ed.; Oliver & Boyd: Edimburgh, 1972.

Table 3. Summary of PXRD Results for the Calcined Samples

NiFe		NiFeH			
450	750	450	750	calcd	ascription
	4.808	4.819	4.799	4.806	(111)S
	2.943	2.940	2.940	2.943	(220)S
	2.509	2.513	2.507	2.510	(311)S
2.419	2.413	2.414	2.407	2.403	(222)S, (101)O
2.341	2.342	2.341	2.341		Al sample holder
2.088	2.088	2.086	2.084	2.090	(400)S, (012)O
2.029	2.027	2.029	2.027		Al sample holder
	1.700	1.699	1.699	1.699	(422)S
	1.603	1.602	1.602	1.602	(511)(333)S
1.476	1.476	1.473	1.473	1.472	(440)S, (110)O
1.432	1.432	1.432	1.432		Al sample holder

S = $NiFe_2O_4$ spinel; O = NiO. Positions of the lines are given in Å.

It should be concluded that in both samples prepared in the present study, the solids display the hydrotalcite-type structure; hydrothermal treatment develops, in addition, an impurity identified as a $NiFe_2O_4$ spinel. The *c* and *a* parameters are close to those reported in the literature for hydrotalcite materials with first transition cations in the layers and carbonate in the interlayer.[26]

The PXRD diagrams for the calcined samples are also shown in Figure 1. The crystallographic phases identified, as well as the positions of the maxima recorded, are summarized in Table 3.

As shown by these data, hydrothermal treatment leads to a different evolution in the nature of the phases existing in both samples. Calcination at 450 °C of sample NiFe leads exclusively to crystallization of NiO, with the rock salt structure, for which the main diffraction maxima are recorded at 2.419, 2.088, and 1.476 Å and are due to diffraction by planes (101), (012), and (110), respectively. The sharp peaks at 2.341, 2.029, and 1.432 Å are due to the aluminum sample holder used to record these diffractograms. While a crystalline phase has been identified, thus (at least partially) accounting for the location of the Ni(II) ions, the location of the trivalent cations remains unknown. These Fe(III) ions may be substituing Ni(II) ions on the NiO lattice or forming amorphous or well-dispersed phases, not detected by X-ray diffraction, in a similar way as described by several authors for Ni−Al and Mg−Al hydrotalcites calcined at 450 °C.[26,33−35]

The diagram for sample NiFeH-450 shows sharper peaks due to the spinel. From comparison of the intensities of these peaks with those reported in the JCPDS tables, it can be concluded that the peaks recorded at 2.414, 2.086, and 1.473 Å are more intense than expected; this can be, however, due to the fact that in these positions diffraction by the NiO structure is also expected. Actually these three peaks are rather broad and their shape is similar to that of the peaks recorded in these same positions in the diagram of sample NiFe-450, and on the other hand, formation of NiO is expected, because as in the parent hydrotalcite the Ni:Fe ratio (2.97) was much larger than that existing in

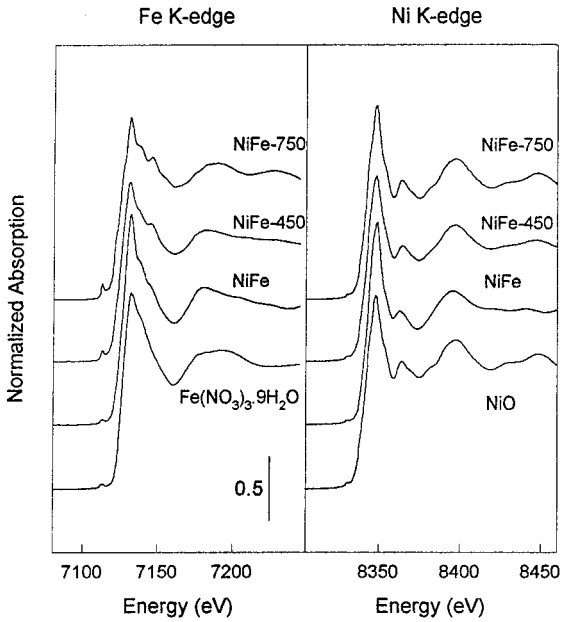

Figure 2. Fe and Ni K-edge XANES for the original NiFe sample and for the same sample calcined at 450 and 750 °C. XANES spectra recorded for selected reference compounds have been included for comparison.

the stoichiometric spinel (0.5). As a consequence, the Ni in excess above that needed to form the spinel crystallizes as NiO.

The diagrams recorded after submitting the samples to calcination at 750 °C are rather similar. Peaks due to NiO and $NiFe_2O_4$ are recorded, and the ascription has been also included in Table 3. The only difference is the larger intensities of the peaks recorded for sample NiFeH-750, suggesting the presence of better crystallized phases in this case.

X-ray Absorption Spectra. To determine in the location of the cations in the parent samples and in those submitted to calcination, X-ray absorption spectra have been recorded at both Ni and Fe K-edges. The study has been limited to sample NiFe and those obtained from its calcination, as PXRD has shown the formation of crystalline spinel in sample NiFeH.

The near-edge region of the spectra (XANES) at both absorption edges is shown in Figure 2, which also includes for comparison data obtained for selected reference compounds. The Fe K-edge XANES for original NiFe is very similar to that recorded for $Fe(NO_3)_3 \cdot 9H_2O$, where Fe(III) cations are in octahedral oxygen coordination. On the other hand, Ni K-edge XANES for original NiFe is very similar to that of NiO, with the rock salt structure, i.e., Ni(II) cations octahedrally coordinated by oxygen atoms. When the sample is calcined at increasing temperatures, Ni K-edge XANES shows only minor changes, showing that Ni(II) cations are still located in octahedral holes, while Fe K-edge XANES spectra show a different postedge structure and develop a weak preedge peak suggesting that at least some Fe(III) cations have moved to tetrahedral sites.

Ni and Fe K-edge EXAFS oscillations for samples NiFe and NiFe-*T* (*T* = 450 and 750 °C) and their associated Fourier transforms (FT) are shown in Figures 3−5. Data for crystalline NiO and $Fe(NO_3)_3 \cdot 9H_2O$ are also included in these figures. As shown in Figure 4, two distinct maxima appear for NiO at 1.5 and 2.7 Å in

(33) Ross, J. R. H. In *Catalysis Specialists Periodical Reports*; Bond, G. C., Webb, G., Eds.; The Royal Society of Chemistry: London, 1985; Vol. 8, p 1.
(34) Rey, F.; Forniés, V.; Rojo, J. M. *J. Chem. Soc., Faraday Trans.* **1992**, *88*, 223.
(35) Sato, T.; Kato, K.; Endo, T.; Shimada, M. *Reactivity Solids* **1986**, *2*, 253.

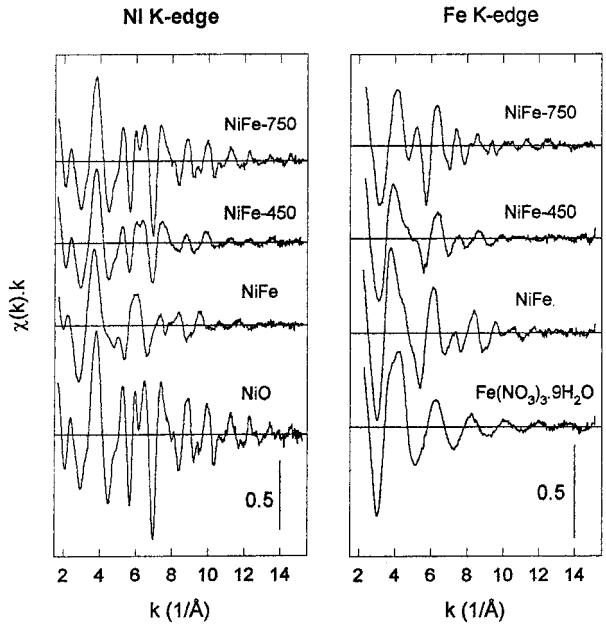

Figure 3. Fe and Ni K-edge EXAFS oscillations for the original NiFe sample and for the same sample calcined at 450 and 750 °C. EXAFS oscillations recorded for selected reference compounds have been included for comparison.

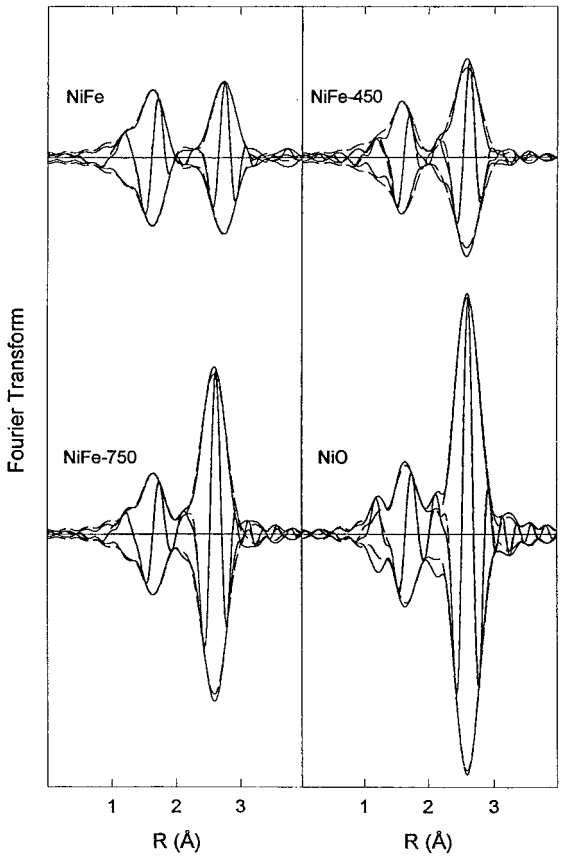

Figure 4. Ni K-edge EXAFS: modulus and imaginary part of the k^3-weighted Fourier transform for the original NiFe sample and for the same sample calcined at 450 and 750 °C. Data for crystalline NiO have been included for comparison (solid lines, experimental data; dashed lines, best fit functions according to parameters in Table 4; $\Delta k = 3-14$ Å^{-1} in all the Fourier transforms).

the FT without phase shift correction of their Ni K-edge EXAFS oscillations. According to the structure of this

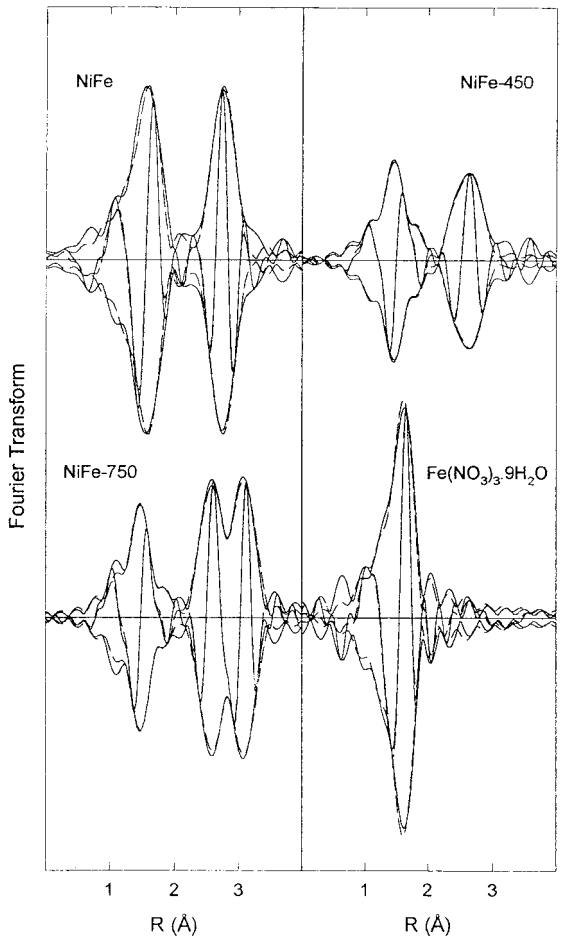

Figure 5. Fe K-edge EXAFS: modulus and imaginary part of the k^3-weighted Fourier transform for the original NiFe sample and for the same sample calcined at 450 and 750 °C. Data for crystalline $Fe(NO_3)_3 \cdot 9H_2O$ have been included for comparison (solid lines, experimental data; dashed lines, best fit functions according to parameters in Table 4; $\Delta k = 3-14$ Å^{-1} in all the Fourier transforms).

compound,[36] Ni(II) cations are surrounded by 6 oxygen atoms at 2.09 Å and 12 Ni(II) cations that form the second coordination shell at 2.95 Å. These two coordination shells were Fourier-filtered from EXAFS data (forward FT, k^3-weighted, $\Delta k = 2.5-15.1$ Å^{-1}; inverse FT, $\Delta R = 0-3.5$ Å). In agreement with structural data, an excellent fit of the EXAFS data is obtained when considering two shells with the coordination parameters included in Table 4. Meanwhile, in $Fe(NO_3)_3 \cdot 9H_2O$ the first coordination shell is formed by six oxygen atoms at 1.98 Å,[37] and the FT without phase shift correction of its Fe K-edge EXAFS oscillations shows a single maximum at ca. 1.5 Å (Figure 5). This maximum was Fourier-filtered (forward FT, 2.5−14.9 Å^{-1}; inverse FT, 0−2.5 Å) and fitted with a single coordination shell formed by six oxygen atoms at 1.99 Å (Table 4), also in agreement within experimental error with reported structural data. Therefore, the theoretical backscattering amplitude and phase shift functions used to fit Fe−O, Ni−O, and Ni−Ni absorbed backscatterer pairs are adequate. No reference compounds were used to check the theoretical functions calculated for Ni−Fe, Fe−Ni,

(36) Sasaki, S.; Fujino, K.; Tabeuchi, Y. *Proc. Jpn. Acad.* **1979**, *55*, 43.
(37) Hair, N. J.; Beattie, J. K. *Inorg. Chem.* **1977**, *16*, 245.

Table 4. Structural Parameters Fitted to EXAFS Oscillations[a]

		Ni K-edge				Fe K-edge			
sample	neighbor	N	$\Delta\sigma^2 \times 10^3$ (Å^2)	R (Å)	$\Delta E°$ (eV)	N	$\Delta\sigma^2 \times 10^3$ (Å^2)	R (Å)	$\Delta E°$ (eV)
NiO	O	6.1	3.9	2.09	3.1	–	–	–	–
	Ni	12.4	4.5	2.94	7.1	–	–	–	–
$Fe(NO_3)_3 \cdot 9H_2O$	O	–	–	–	–	6.0	3.7	1.99	3.0
NiFe	O	6.2	4.7	2.04	6.9	6.4	5.9	2.00	5.4
	M	6.2	6.7	3.08	6.4	5.9	7.0	3.09	4.5
NiFe-450	O	5.9	6.0	2.04	8.4	1.9	1.2	1.89	2.2
						2.9	3.4	2.02	8.0
	M	8.9	8.6	2.95	8.2	6.2	13.5	2.99	5.0
NiFe-750	O	6.0	5.3	2.07	4.3	1.9	0.7	1.89	−0.2
						3.0	3.8	2.01	6.8
	M	10.8	6.0	2.94	8.0	3.9	8.1	2.95	6.8
		1.3	6.7	3.46	8.0	7.7	7.1	3.44	10.2

[a] Fit ranges: $\Delta k = 3-14$ Å^{-1}; $\Delta R = 0-3.5$ Å. Data for the first two coordination shells were Fourier filtered (forward FT, k^3-weighted, $\Delta k = 2.5-15$ Å^{-1}; $\Delta R = 0-3.5$ Å). Estimated errors in coordination numbers (N) and shell radii (R) are ±10−15% and ±1−2%, respectively.

or Fe−Fe absorber backscatterer pairs, since all of them are nearly identical to that obtained for Ni−Ni pairs, as expected, due to the close atomic numbers of Ni and Fe. It should be noted here that this fact prevented us from any attempt to distinguish between Ni and Fe as backscatterers when both types of atoms were present in the samples, and have limited us to define coordination numbers and shell radii for metallic (M) shells (M = Ni and/or Fe).

For the original NiFe sample, FTs without phase shift correction obtained at Ni and Fe K-absorption edges show two distinct maxima close to 1.5 and 3.0 Å (Figures 4 and 5). The best fit to both EXAFS spectra was achieved with six oxygen atoms in the first coordination shell of the transition metal cation and six metal cations in a second coordination shell, according to the expected coordination numbers for cations in the brucite-like layers.[38] On comparing the M−O (M = Ni or Fe) distances calculated at the Ni and Fe edges (see Table 4), a slight decrease has been observed for the trivalent cation Fe(III). This effect has been previously reported by us for hydrotalcites containing Co(II) and Cr(III) in the brucite-like layers[38] and suggests distortions in the layers because of the different size of the cations. This shortening is, however, small (0.04 Å) and close to the experimental error in shell radii (1−2%) for the NiFe sample, due to the small difference between the ionic radii of Fe(III) and Ni(II) cations (0.65 and 0.70 Å, respectively).[39] M−M distances determined from the EXAFS spectra (3.08−3.09 Å) arise from [MO_6] octahedra (M = Ni, Fe) that share a vertex in the brucite-like layers and agree with the value for the *a* parameter found for the NiFe sample by PXRD (3.078 Å).

A qualitative inspection of EXAFS data for calcined samples indicates that the intensity of the maximum associated with the first coordination shell at the Ni K-edge remains nearly constant after calcination (Figure 4), while at the Fe K-edge it decreases in a significant amount when going from the original sample to the calcined ones (Figure 5). Coordination parameters yielding a best fit of EXAFS data up to 3.5 Å in the *R*-space are summarized in Table 4, while best fit functions are compared with experimental FT data in Figures 4 and 5. Results obtained from Ni K-edge EXAFS show that, also for the calcined samples, the total number of oxygen atoms in the first coordination shell of Ni cations is six, within experimental error. A second shell Ni−M (M = Ni or Fe) distance of 2.94−2.95 Å is obtained, the coordination number at this distance increasing when the calcination temperature increases.

Meanwhile, when only one Fe−O first shell distance is included in the best fit to Fe K-edge EXAFS data for both calcined samples (shell radii $R = 1.92$ Å, coordination number $N = 4.3-4.5$), a lack of agreement between experimental and theoretical data is observed in the 0−2 Å range. The fit is improved by including two oxygen subshells at 1.89 and 2.02 Å, with coordination numbers 1.9 and 2.9−3.0, respectively. When going from the one Fe−O shell model to the two Fe−O subshells model, k^3 variances decrease from 7.1% to 2.9% for NiFe-450 and from 3.4% to 1.6% for NiFe-750, while the goodness of fit parameter, ϵ_ν^2, decreases from 15 to 11 for NiFe-450 and from 11 to 10 for NiFe-750, indicating that the two subshell model is significant. Second shell coordination parameters for iron detect about 6 M neighbors (M = Ni or Fe) at 2.99 Å in the NiFe-450 sample, and near 12 M neighbors, 3.9 at 2.94, and 7.7 at 3.44 Å, for the NiFe-750 samples.

Coordination parameters for the cations obtained from EXAFS data for NiFe-750 are consistent with the detection by PXRD for this sample of a mixture of NiO and $NiFe_2O_4$ phases. Ni(II) cations occupy octahedral holes in NiO and in $NiFe_2O_4$, an inverse spinel (inversion degree 0.5),[40] where all divalent cations are in octahedral holes and trivalent cations are homogeneously distributed between octahedral and tetrahedral holes. Considering the composition of the starting hydrotalcite (Ni/Fe = 2.4) and that expected for the spinel (Ni/Fe = 0.5), all Fe(III) cations can enter the spinel phase, while only 20% of Ni(II) cations could form the spinel, the excess appearing as NiO. According to crystallographic data for these compounds,[36,41] expected Ni−O distances in the octahedral hole are 2.04−2.09 Å, while Fe−O distances are 1.89 Å at the tetrahedral hole and 2.04 Å at the octahedral one. For a half of the Fe(III) cations in each type of hole, we expect average coordination numbers of 2.0 and 3.0 at the shortest and longest Fe−O distances, these values being close to those found from the analysis of EXAFS data for NiFe-750, thus showing that in this sample all Fe(III) cations are distributed between octahedral and tetahedral holes, as in crystalline $NiFe_2O_4$.

Regarding M−M shells, [NiO_6] octahedra in NiO share all edges with other octahedra, the crystallographic Ni−Ni distance being 2.95 Å and the expected coordination number 12. In the spinel phase (see Scheme 1a), [MO_6] octahedra share edges with other six octahedra, and vertices with six [MO_4] tetrahedra, while

(38) Del Arco, M.; Galiano, M. V. G.; Rives, V.; Trujillano, R.; Malet, P. *Inorg. Chem.* **1996**, *35*, 6362.

(39) Huheey, J. E.; Keiter, E. A.; Keiter, R. L. *Inorganic Chemistry: Principles of Structure and Reactivity*, 4th ed.; Harper Collins College Publishers: New York, 1993.

(40) Wells, A. F. *Structural Inorganic Chemistry*, 5th ed.; Oxford Science Publications: Oxford, 1984; p 593 ff.

(41) Subramanyan, K. N. *J. Phys. C* **1971**, *4*, 2266.

Scheme 1. (a) Fragment of the Spinel Structure (111 planes) Showing the Distribution of Cations between Octahedral and Tetrahedral Holes[a] and (b) Defective Tetrahedral Site Accounting for the Observed M−M Distance Close to 3 Å[b]

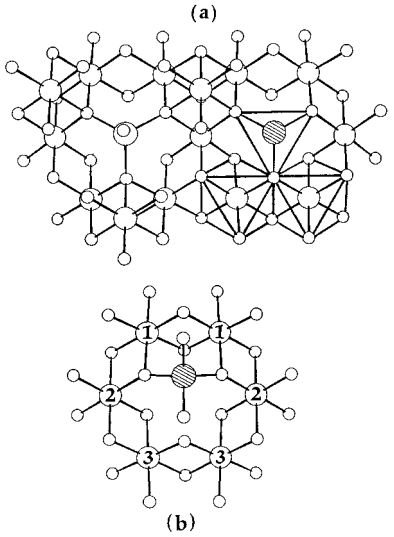

[a] Two edge-sharing octahedra and a cation in the tetrahedral hole (dashed) sharing vertices with octahedral holes have been marked. [b]Small circles, oxygen anions; large circles, M cations).

all [MO_4] tetrahedra share each of their four vertices with three [MO_6] octahedra. M−M distances determined from crystallographic data[41] for $NiFe_2O_4$ are 2.95 Å for edge-sharing octahedra and 3.46 Å for vertex-sharing tetrahedron−octahedron pairs. Therefore, for half of the Fe(III) cations in tetrahedral holes and the other half in octahedral ones, average coordination numbers at the second shell of iron should be 3.0 at 2.95 Å and 9.0 at 3.46 Å. Experimental values of Fe−M shell radii derived from Fe K-edge EXAFS data for NiFe-750 are in good agreement with those expected for the inverse spinel structure, although coordination numbers at these distances (3.9 at 2.95 Å and 7.7 at 3.44 Å) are respectively larger and lower than the expected values for a well-crystallized inverse spinel. On the other hand, a coordination number of 10.8 is obtained for Ni(II) at the characteristic octahedron−octahedron distance of 2.94 Å, while neighbors at 3.46 Å do not yield a distinct signal in the radial distribution function derived for Ni cations from Ni K-edge EXAFS data for NiFe-750. It should be noted that the maximum amount of Ni(II) included in the spinel phase is 20%, and the 3.46 Å Ni−M distance is absent in the oxide. For a composition of 20% $NiFe_2O_4$ and 80% NiO, and average coordination number of 1.2 can be calculated at this Ni−M distance and, actually, the fit of Ni K-edge EXAFS data for NiFe-750 can be slightly improved by adding 1.3 M neighbors at 3.46 Å, k^3-variance decreasing from 1.0% to 0.6%.

Most interesting results are obtained for NiFe-450. As stated above, the PXRD data for this sample only detect an ill-crystallized NiO phase, accounting at least partially for the location of the Ni(II) ions, while diffraction lines for any compound containing iron are absent, the technique being unable to yield any information about the location of Fe(III) cations in this sample. Coordination numbers and shell radii at the first coordination shell of Ni and Fe, derived from EXAFS data for NiFe-450, are equal within experimental error to those obtained for NiFe-750. Therefore, the distribution of both cations between tetrahedral and octahedral holes in the sample calcined at low temperature is the same as that described for the sample calcined at 750 °C, with all Ni(II) cations in octahedral holes and half of the Fe(III) cations in tetrahedral holes and the other half in octahedral ones. This distribution of cations discards the formation of a Ni(II)−Fe(III) oxide solid solution with the rock salt structure, where Fe(III) substitutes for Ni(II) in the octahedral holes of the oxygen framework. Half of iron cations are in tetrahedral oxygen coordination, thus suggesting that iron could be forming an amorphous oxide phase with a structure related to inverse spinels, such as $NiFe_2O_4$ or γ-Fe_2O_3. Although small clusters of these spinel-like oxide had to be assumed, since they are not detected by PXRD after calcination at 450 °C, these clusters would yield Fe−M shell radii at the second coordination shell of iron characteristic of the spinel structure and close to 3 and 5 Å.

Experimental coordination parameters for Fe−M shells (M=Fe or Ni), derived from Fe K-edge EXAFS data for NiFe-450, detected 6.2 M neighbors at 2.99 Å, close to the characteristic distance between ions in edge-sharing octahedra, although the coordination number at this distance is twice the average value expected for Fe(III) cations in the inverse spinel. Moreover, Fe/Ni neighbors at 3.44 Å, expected for vertex-sharing tetrahedron−octahedron pairs in the spinel structure, are absent within the detection limit of the technique. Therefore, although half of the Fe(III) cations have entered tetrahedral holes in this sample, the location of these tetrahedra is different from that shown in Scheme 1a for the spinel structure, and the formation of small clusters of $NiFe_2O_4$ or γ-Fe_2O_3 can be discarded.

It should be noticed that, even after calcination of the NiFe sample at 750 °C, coordination numbers at 2.95 and 3.44 Å are still larger and lower, respectively, than the expected values for a well-crystallized inverse spinel. Data reported in the literature for ill-crystallized materials formed after thermal decomposition of other layered double hydroxides also support the presence of the same type of defect site. Thus, structural data obtained from EXAFS for thermally decomposed Co(II)−Cr(III) hydrotalcites[38] found more Co-M bonds at 2.9−3.0 Å than the values expected from the exclusive formation of stoichiometric compounds. Also Belloto et al.[42] reported for partially decomposed Mg(II)−Ga(III) samples the absence, up to 900 °C, of the Ga−M shell radii close to 3.4−3.5 Å, characteristic of Ga−Mg and Ga−Ga distances in the $MgGa_2O_4$ spinel structure. These authors postulate that upon dehydration the layered structure is preserved, but trivalent cations diffuse out of the layer, leave vacant their formerly occupied octahedral position, and assume a tetrahedral coordination with three oxygen atoms of the layer and one apical oxygen at the interlayer. This coordination is similar to that found in the spinel (see Scheme 1a), and therefore, it does not explain the absence of the M−M distance at 3.4 Å between the cation in tetrahedral coordination and the vertex-sharing octahedrally coordinated cations. At higher decomposition tempera-

(42) Belloto, M.; Rebours, B.; Clause, O.; Lynch, J.; Bazin, D.; Elkaim, E. *J. Phys. Chem.* **1996**, *100*, 8535.

tures, a spinel-like phase is proposed by Belloto et al.,[42] with Ga tetrahedrally coordinated and Mg octahedrally coordinated. These authors propose that the absence of Ga−Ga distances close to 3.5 Å predicted by such a model could be due to a concentration of tetrahedral Ga ions higher than that found in the crystalline spinel, thus forcing [GaO_4] tetrahedra to share corners and reducing the Ga−Ga distance. However, this model does not explain the absence of the Ga−Mg distance at 3.4 Å, also characteristic of a spinel structure.

Since EXAFS data only yield for NiFe-450 one M(III)−M distance at ca. 3 Å, the coordination number found at this distance being about six and decreasing at higher calcination temperatures, experimental data suggest that M neighbors at the second coordination shell of a cation in the tetrahedral hole should be also close to 3 Å. A tentative location for the defect tetrahedral site is shown in Scheme 1b: during decomposition of the sample the trivalent cation has left its octahedral position in the brucite layer, diffusing into the interlayer space, and assumes a tetrahedral coordination with two oxygen atoms from the layer and two from the interlayer space, one of its C_2 axes being perpendicular to the octahedral layer. The structure of the proposed cluster is related to the structure of the original sample and also related to the structure of the spinel that is formed at higher temperatures. Considering other structural parameters identical to those reported for the spinel structure, M neighbors for a cation located in the proposed tetrahedral site appear at 3.07, 3.73, and 4.30 Å (labeled as 1, 2, and 3, respectively, in Scheme 1b), thus accounting for the absence of a M−M shell radius of 3.44 Å and for the observed increase in the average coordination number at ca. 3 Å.

Specific Surface Area. The values calculated by nitrogen adsorption at −196 °C are given in Table 1. As previously observed for other hydrotalcite-type solids,[43] hydrothermal treatment leads to a sharp decrease in the specific surface area of the samples. This change should be related to the better crystallinity of the hydrothermally treated sample.

Upon calcination, the specific surface area for sample NiFe-450 decreases to 64 m^2/g, while for NiFeH-450 it increases to 55 m^2/g. Finally, calcination at 750 °C leads to the same value for the specific surface area (13 m^2/g), in agreement with the similar features concluded by PXRD and XAS studies.

FT-IR Spectroscopy. The spectra for the original and the calcined samples are included in Figure 6. The broad band between 4000 and 3000 cm^{-1} is due to the OH stretching mode; the broadness of this band for the original hydrotalcites arises from the wide number of different O−H bonds existing in these samples, namely, hydroxyl groups in the brucite-like layers (bonded to Ni(II) or Fe(III) cations) and hydroxyl groups from interlayer water molecules; in addition, all these groups are linked by hydrogen bonds of different strengths. The broad shoulder around 3000 cm^{-1} has been ascribed[44] to the OH stretching mode of hydroxyl groups hydrogen-bonded to interlayer carbonate anions.

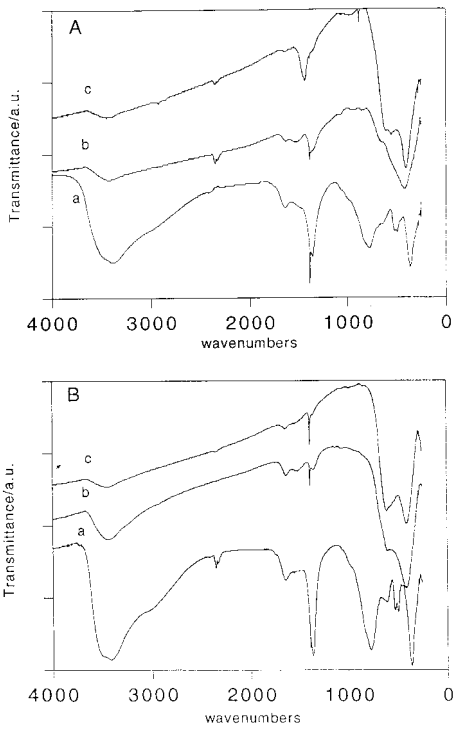

Figure 6. FT-IR spectra of samples: (A) NiFe, and (B) NiFeH corresponding to the original sample (a) and the sample calcined at 450 °C (b) and 750 °C (c).

The sharp absorption close to 1385 cm^{-1} is due to mode ν_3 of the interlayer carbonate species. The shift of this band from the position for free carbonate anion is related to the restricted symmetry in the interlayer space,[45] which decreases its symmetry from D_{3h}, an effect similar to that observed in calcite (symmetry D_3) and aragonite (C_s), two crystalline forms of calcium carbonate.[46,47] The band close to 1625 cm^{-1} is due to the bending mode of water molecules in the interlayer space, although this band has been also related to the presence of bicarbonate species.[48,49] Bands at lower wavenumbers are due to other modes of bicarbonate and to vibrations implying M−O, M−O−M, and O−M−O bonds in the layers.

The spectra of the calcined samples are different. The bands due to hydroxyl groups and water molecules are very much weaker, probably because in these samples water only exists adsorbed on the external surface of the particles. The weak band, still recorded close to 1400 cm^{-1}, should be due to adsorbed carbonate species, and the bands below 1000 cm^{-1} should be due to M−O, M−O−M, and O−M−O related modes.

Thermogravimetric and Differential Thermal Analyses. The traces for the original hydrotalcites are shown in Figure 7. The DTA curve for sample NiFe shows a first, intense endothermic effect at 242 °C, with a shoulder at 150 °C, followed by a second endothermic

(43) Labajos, F. M.; Rives, V.; Ulibarri, M. A. *J. Mater. Sci.* **1992**, *27*, 1546.
(44) Kruissink, E. C.; Van Reijden, L. J.; Ross, J. R. H. *J. Chem. Soc., Faraday Trans. 1*, **1981**, *77*, 649.
(45) Hernández-Moreno, M. J.; Ulibarri, M. A.; Rendón, J. L.; Serna, C. *J. Phys. Chem. Miner.* **1985**, *12*, 34.
(46) Nakamoto, K. *Infrared and Raman Spectra of Inorganic and Coordination Compounds*, 4th ed.; J. Wiley & Sons: New York, 1986.
(47) Rives-Arnau, V.; Munuera, G.; Criado, J. M. *Spectrosc. Lett.* **1979**, *12*, 733.
(48) Serna, C. J.; White, J. L.; Hem, S. L. *Clays Clay Miner.* **1977**, *25*, 384.
(49) Serna, C. J.; White, J. L.; Hem, S. L. *Soil Sci. Soc. Am. J.* **1977**, *41*, 1009.

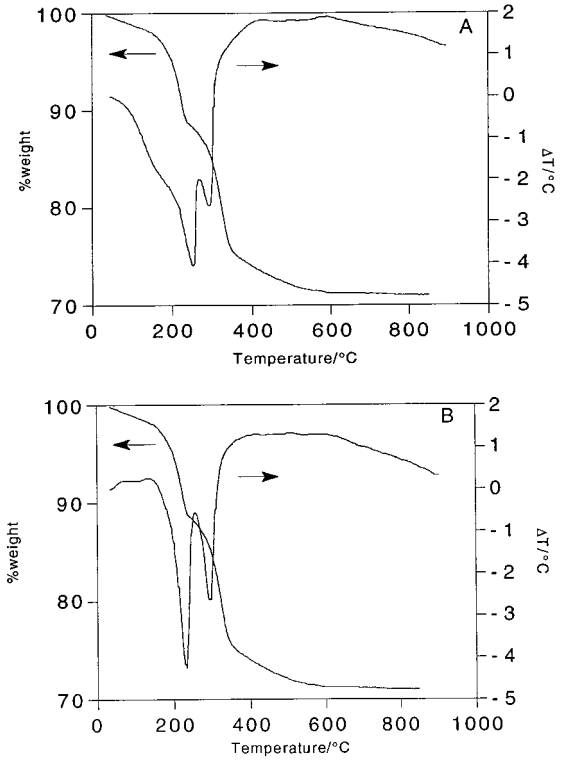

Figure 7. DTA and TG traces of (A) NiFe and (B) NiFeH recorded in air.

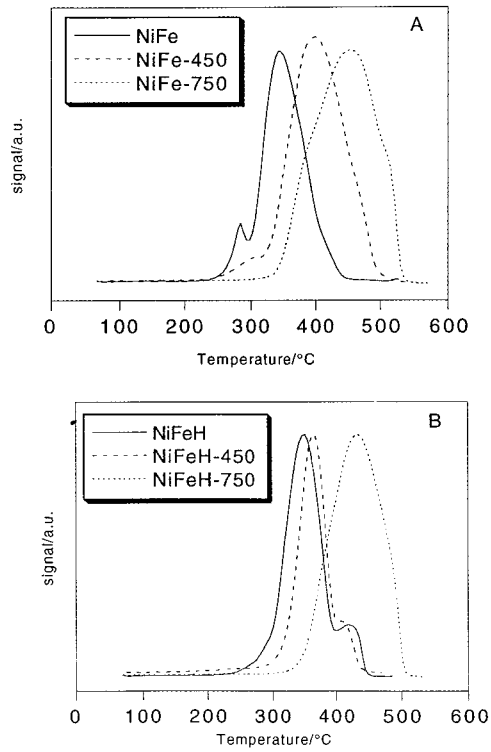

Figure 8. Temperature-programmed reduction profiles of samples (A) NiFe and (B) NiFeH.

effect at 301 °C. The first should indicate the presence of water molecules weakly held, lost before the first main endothermic effect.[50] Such a shoulder is not recorded for sample NiFeH, while the main endothermic effects are recorded at the same temperatures as for sample NiFe, although for the sample submitted to hydrothermal treatment, the peaks are sharper and symmetric. This difference may be due to the larger crystallinity of sample NiFeH than of sample NiFe (as concluded from the sharpness and intensity of the PXRD diffraction peaks; see Figure 1) and to a lower amount of weakly held water (probably physisorbed), due to the lower specific surface area of the hydrothermally treated sample.

The TG diagrams show two weight losses for which the inflection points coincide with the temperatures corresponding to the minima in the DTA traces. According to data reported elsewhere,[51] the first weight loss corresponds to removal of interlayer water molecules, while the second weight loss is due to dehydroxylation of the brucite-like layers and carbon dioxide removal, from interlayer carbonate anions. In agreement with the DTA data, the TG curve for sample NiFe in the low-temperature range shows a less marked decrease, probably corresponding to removal of physisorbed water. The total weight loss was 34% for sample NiFe and 30% for sample NiFeH. From the total weight loss and assuming a final composition of the solids described as $m\mathrm{NiO}\cdot n\mathrm{Fe_2O_3}$, the water content in the interlayer (see Table 1) has been calculated. The difference between both samples could be due to the existence of physisorbed water in sample NiFe, accounting, as indicated above, for the weak shoulder recorded in its DTA trace before the first main endothermic effect. Nevertheless, the amount of interlayer water molecules is in both cases below the maximum expected assuming a close-packing of the hydroxyl groups in the brucite-like layers and a close packing of carbonate anions and water molecules in the interlayer space.

Temperature-Programmed Reduction. As, in many cases, the hydrotalcites are used as precursors for catalysts, we have investigated the reducibility of our hydrotalcites, to assess the effect of hydrothermal and calcination treatments. This technique has been successfuly applied to study reducibility of cations in hydrotalcites.[21]

The curves recorded for both sets of samples are shown in Figure 8. A single reduction peak is recorded in all cases, although some weak shoulders are recorded for some samples.

Ni(II) is reduced during TPR analysis of a Ni−Al hydrotalcite[21] in a single step, the maximum of the reduction peak being recorded at 391 °C, while Fe(III) in the brucite-like layers of a Zn−Al−Fe hydrotalcite[7] is reduced at 380 °C.

In our case, the main reduction maximum for both NiFe and NiFeH samples is recorded at 347 °C. It is also observed that the position of the maximum shifts toward higher temperatures as the precalcination temperature of the sample is increased.

For sample NiFe a weak, sharp peak is recorded before the main reduction maxium, at 285 °C. This can be tentatively ascribed to the presence of a small amount of Ni^{3+} species in the external layers of the solids and that formed during the TPR experiment, as no evidence for Ni^{3+} was concluded from XAS study of the sample; the intensity of this peak decreases with the calcination temperature; it is only a weak shoulder

(50) Miyata, S. *Clays Clay Miner.* **1975**, *23*, 369.
(51) Del Arco, M.; Rives, V.; Trujillano, R. *Stud. Surf. Sci. Catal.* **1994**, *87*, 507.

for sample NiFe-450 and is absolutely absent in the profile recorded for sample NiFe-750.

On the other hand, the reduction profile of sample NiFeH does not show this weak reduction maximum at low temperature, probably because of its much lower specific surface area. On the contrary, a weak shoulder is recorded *above* the main reduction maximum, at 421 °C. The position of this maximum coincides with that of the main reduction peak for sample NiFeH-750, where PXRD and other techniques have demonstrated the presence of $NiFe_2O_4$ spinel. So, we can assume that this peak is due to reduction of cations in the spinel existing in the hydrothermally treated sample.

So, we should conclude that both Ni and Fe are reduced in a single step in all six samples here studied. The reduction temperature increases as the calcination temperature does, and reduction of surface Ni(III) species (in sample NiFe) and of crystalline $NiFe_2O_4$ spinel (in sample NiFeH) are clearly distinguished.

Conclusions

In the present study a layered double hydroxide with the hydrotalcite-like structure has been obtained by coprecipitation; hydrothermal treatment leads to formation of a coproduct, identified by PXRD as the $NiFe_2O_4$ spinel.

Upon calcination at 450 °C of the sample not submitted to hydrothermal treatment, NiO is identified as the single crystalline phase, the $NiFe_2O_4$ spinel being formed after calcination at 750 °C. In this sample all Ni(II) cations are octahedrally coordinated by oxygen anions, while Fe(III) cations are homogeneously distributed between octahedral and tetrahedral holes. Coordination parameters at the first and second coordination shells of Ni(II) and Fe(III) agree with formation of 20% NiO and 80% $NiFe_2O_4$, in agreement as well with the chemical composition and Ni/Fe ratio in this solid. For sample calcined at 450 °C, Ni(II) and Fe(III) cations have the same distribution between tetrahedral and octahedral holes than that found in the $NiO/NiFe_2O_4$ mixture formed at 750 °C. This results discards the formation of a Ni(II)−Fe(III) oxide solid solution with the same structure as NiO, the only crystalline phase detected by PXRD at 450 °C, and indicates that Fe(III) is forming an amorphous phase at this temperature. XAS results indicate that the second coordination shell of Fe(III) cations after thermal treatment at 450 °C is different from that expected for a spinel phase, and the Fe−M (M = Fe and/or Ni) distance of 3.44 Å characteristic of Fe(III) cations in tetrahedral sites at the spinel structure is absent. This result discards the presence in the amorphous phase of small nuclei with a spinel-like structure. Taking into account coordination parameters calculated from XAS data, a tentative structure for the cluster present in the amorphous phases is proposed.

Upon temperature-programmed reduction, both cations are reduced in a single step, although this shifts to higher temperatures when the spinel is present. Reducibility of the mixed oxides obtained at intermediate temperatures (450 °C, i.e., those potentially interesting as catalysts) depends on the synthesis method of the starting hydrotalcite, as well as on the formation of spinel nuclei during calcination.

Acknowledgment. Finantial support from DGESIC (grant PB96-1307-C03) and Consejería de Educación y Cultura de la Junta de Castilla y León (grant SA45/96) is acknowledged. Thanks are also given to LURE (Orsay, France) for facilities for recording the XAS spectra.

CM9804923